Effect of small asymmetries on axisymmetric stenotic flow

Martin D. Griffith[1],†, **Thomas Leweke**[2], **Mark C. Thompson**[1] **and Kerry Hourigan**[1]

[1]Fluids Laboratory for Aeronautical and Industrial Research (FLAIR), Department of Mechanical and Aerospace Engineering & Division of Biological Engineering, Monash University, Melbourne, Victoria 3800, Australia

[2]Institut de Recherche sur les Phénomènes Hors Equilibre (IRPHE), UMR 7342 CNRS, Aix-Marseille Université, 13384 Marseille, France

Flow through axisymmetric and eccentric sinuous stenoses is investigated numerically, for Reynolds numbers up to 400. The eccentricity consists of an offset of the stenosis throat. A range of stenosis eccentricity is tested; the wake flow is found to be highly sensitive to small eccentricities in the stenosis geometry, even with stenosis offsets of the order of the machining precision of experimental test-sections. Comparisons are made between the numerically simulated flow through stenoses with small eccentricities and results from the literature of non-axisymmetric flows through nominally axisymmetric geometries. The effect of distortion to the inlet Poiseuille velocity profile is also investigated and found to have a significantly less severe effect on the downstream wake flow than geometric eccentricity.

Key words: instability control, separated flows, wakes/jets

1. Introduction

Ahmed & Giddens (1983) performed an experimental investigation of the flow through an axisymmetric stenosis, defined by a sinuous constriction of an axial length of two pipe diameters. Most of the stenotic fluid dynamics studies in the literature since have used this stenosis geometry (Sherwin & Blackburn 2005; Varghese, Frankel & Fischer 2007; Vétel *et al.* 2008). The steady base flow consists of a jet emanating from the stenosis throat, surrounded by a long, thin recirculation zone. More recently, Vétel *et al.* (2008) have presented stereoscopic particle image velocimetry (SPIV) data for the problem, thereby providing a detailed three-dimensional description of the flow. In their work, they found that the first instability of the steady axisymmetric base

† Email address for correspondence: martin.griffith@eng.monash.edu.au

flow arises for a critical Reynolds number $Re \approx 250$ and consists of a weak deflection of the jet towards the wall, causing a non-axisymmetric recirculation zone. At higher Reynolds numbers, the deflection becomes stronger, resulting eventually in an unsteady non-axisymmetric flow.

A key point of interest rises from the work of Vétel *et al.* (2008) when considered alongside the earlier work of Sherwin & Blackburn (2005), who performed a numerical study of the same flow. Using linear stability analysis, they predicted the flow to become unstable at a critical Reynolds number $Re_c = 722$ to an instability mode consisting of a deflection of the jet from the centreline of the pipe. The instability mode appears to be the one observed experimentally by Vétel *et al.* (2008); however, there is a large difference between the two critical Reynolds numbers. Vétel *et al.* (2008) suggest in their conclusions that small non-axisymmetric imperfections or perturbations in the experimental setup could account for the early breaking of axisymmetry. Similar discrepancies between experiments and numerical calculation have been observed for the flow in planar and axisymmetric sudden expansions (Fearn, Mullin & Cliffe 1990; Cantwell, Barkley & Blackburn 2010; Sanmiguel-Rojas, del Pino & Gutiérrez-Montes 2010). Sanmiguel-Rojas & Mullin (2012) have investigated the effect of inlet velocity profile perturbations on the wake of axisymmetric sudden expansion flow and found strong similarities with the observed non-axisymmetric flows.

A number of studies have investigated the effect on stenotic flow of non-axisymmetric perturbations to the geometry (Varghese *et al.* 2007) and the inlet velocity profile (Peterson & Plesniak 2008). Peterson & Plesniak (2008) investigated experimentally the effect on stenotic flow of skewed velocity profiles and secondary flow generated by a pipe bend on the main flow features, however on pulsatile stenotic flow. They found that a strong skewing of the velocity profile of the pulsatile inlet significantly reduced the extent of the stenotic jet, forcing it towards the pipe wall. Varghese *et al.* (2007) investigated numerically the steady inlet flow through both the sinuous stenosis used in Sherwin & Blackburn (2005), Peterson & Plesniak (2008) and Vétel *et al.* (2008), and also an eccentric stenosis. The eccentric stenosis consisted of the axisymmetric sinuous stenosis geometry with an added offset to the throat of 5 % of the pipe diameter. They found the flow through the eccentric stenosis to be greatly altered when compared to the flow through the axisymmetric stenosis. The jet attached strongly to the side of the pipe in the direction of the throat offset. They simulated the flow through both geometries for Reynolds numbers $Re = 500$ and 1000, finding in all cases the flow to be steady, except for the eccentric case for $Re = 1000$, where transition to turbulence was observed 5 diameters downstream of the stenosis.

Both the studies of Varghese *et al.* (2007) and Peterson & Plesniak (2008) documented the effect on the flow of a relatively large non-axisymmetric perturbation to the system or boundary conditions. The research presented in this paper seeks to quantify the sensitivity of the stenotic flow to much smaller disturbances, by varying a precisely defined eccentric geometric perturbation. It is hypothesized that such disturbances – even when applied at magnitudes typical of manufacturing tolerances for experiments – are sufficient to lead to substantial asymmetry in the flow.

2. Method

2.1. *Problem definition*

The geometries under consideration in this study are defined in the same way as in Varghese *et al.* (2007). A schematic is shown in figure 1. The coordinate origin is
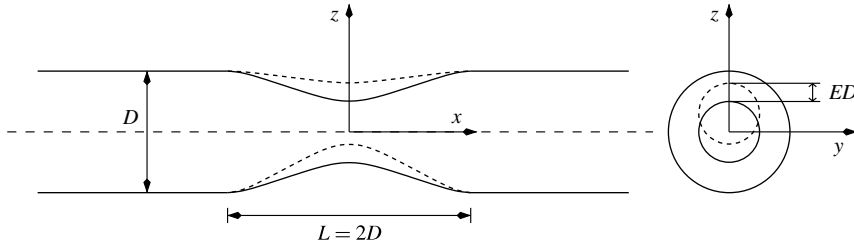
FIGURE 1. Schematic of the geometries under consideration. The dotted curve represents an example eccentric stenosis.

placed on the centreline of the pipe at the axial mid-point (throat) of the stenosis. The stenosis height, $H(x)$, is defined as

$$H(x) = 0.5D[1 - 0.25(1 + \cos(2\pi x/L))], \qquad (2.1)$$

where D is the pipe diameter and L is the axial length of the stenosis. For the sinuous stenoses studied in this paper, $L = 2D$. The cross-stream coordinates of the stenosis surface are then defined as $y_s = H(x)\cos\theta$ and $z_s = H(x)\sin\theta$, where $\theta = \operatorname{atan} z/y$.

The eccentricity of the throat is defined as

$$E_z(x) = 0.5ED(1 + \cos(2\pi x/L)), \qquad (2.2)$$

where E is equal to the stenosis throat offset. The modified z-coordinate is then $z = E_z(x) + H(x)\sin\theta$. The case $E = 0$ represents the base axisymmetric stenosis shape. A range of stenosis eccentricities has been tested, $0 \leqslant E \leqslant 0.05$.

The Reynolds number is defined as

$$Re = \frac{UD}{\nu}, \qquad (2.3)$$

where U is the cross-sectionally averaged velocity in the pipe and ν is the kinematic viscosity. The Reynolds number range tested is $1 < Re < 400$.

2.1.1. *Numerical method*

For the numerical simulations, a three-dimensional hexahedral spectral-element solver is used to solve the incompressible, time-dependent Navier–Stokes equations. It uses the same computational code as used in Griffith *et al.* (2007) and Griffith *et al.* (2008), only re-configured for the three-dimensional hexahedral mesh. The mesh, showing macro-elements, for the axisymmetric case ($E = 0$) is shown in figure 2. Nodes internal to each macro-element are distributed according to Gauss–Legendre–Lobatto quadrature; the accuracy of the simulation can be improved by incrementing the polynomial order, n, of the quadrature. For the flow with $Re = 300$ and eccentricity $E = 0.05$, separate simulations were run with polynomial orders $n = 5, 6, 7$ and 8. The number of node points used in the simulation varies from 115 785 for a polynomial order $n = 5$, to 609 435 for a polynomial order of $n = 8$. The spectral-element method has been shown to converge spectrally with polynomial order (Karniadakis & Sherwin 1999). Cross-stream and axial velocity profiles were examined at various axial stations, with figure 3 showing the results for $x/D = 3.5$. For the simulation with $n = 6$, the maximum variation of u-velocity values was less than 0.3 % of the corresponding value in the $n = 8$ simulation, while the maximum variation of
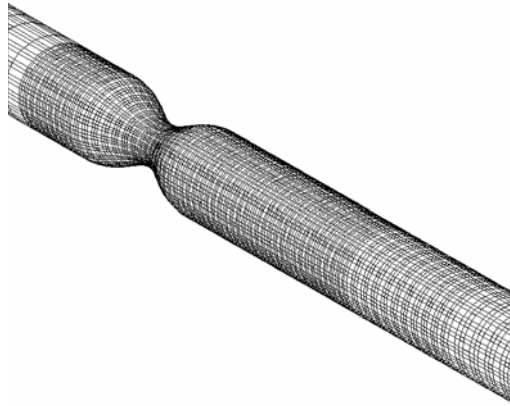
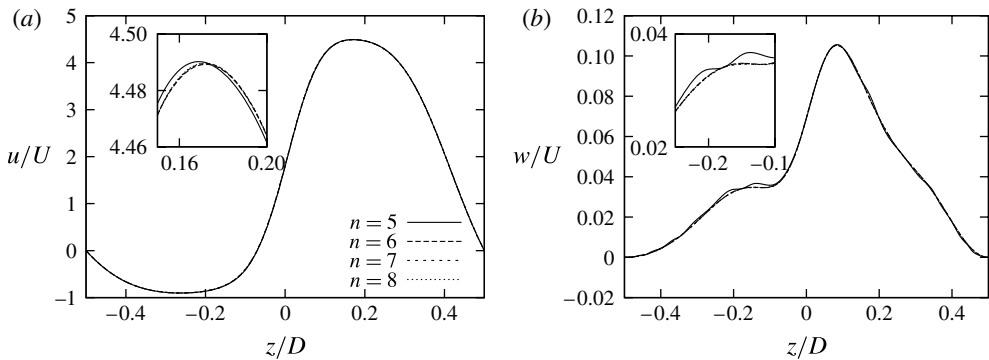FIGURE 2. The mesh used for the axisymmetric case ($E = 0$).

FIGURE 3. Velocity profiles taken at an axial station of $x/D = 3.5$ across the centre of the pipe, for $Re = 300$ and stenosis of eccentricity $E = 0.05$: (*a*) axial velocity, u, (*b*) velocity in the direction of the stenosis offset, w. Inset are plots zoomed on areas where the simulation with the coarsest mesh ($n = 5$) varies most from that with the finest mesh ($n = 8$).

w-velocity values was less than 0.4%. All the results shown in this paper were run with polynomial order $n = 6$.

All simulations were initialized from rest and run until a steady solution was achieved. A Poiseuille inlet profile is prescribed a distance of 6 pipe diameters upstream of the stenosis, while the outlet is placed 25 diameters downstream from the stenosis. Simulations with longer inlet and outlet lengths were run and no change in the near wake of the stenosis was observed, including for cases exhibiting hysteretic behaviour, outlined later in the paper.

3. Results

Figures 4 and 5 present examples of the flows under consideration. From figure 4, for a Reynolds number of 300, the increasing deflection of the flow with stenosis eccentricity is apparent. For an eccentricity of $E = 0.05$, the flow is strongly deflected,
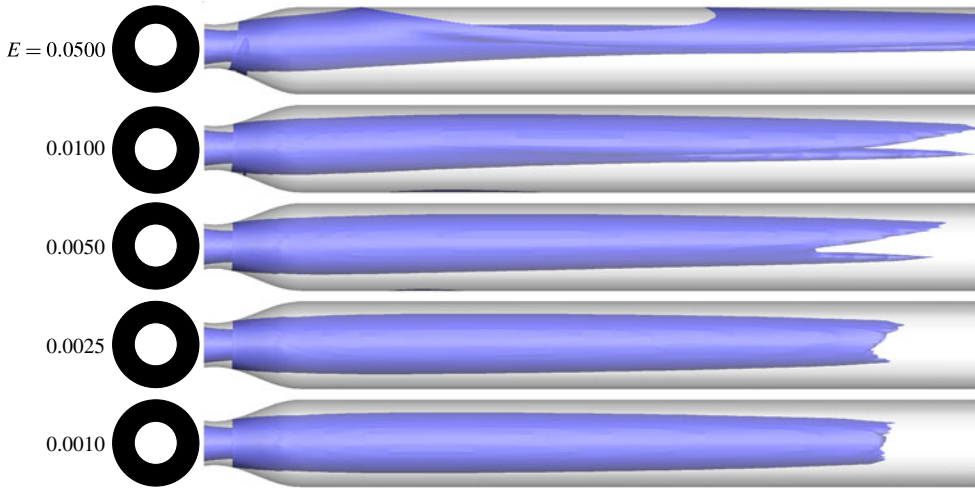
FIGURE 4. Isosurfaces of vorticity magnitude ($|\omega| = 12$) of the flow across a range of stenosis eccentricity, for $Re = 300$. Orthogonal views of the stenosis throat are given for each case.
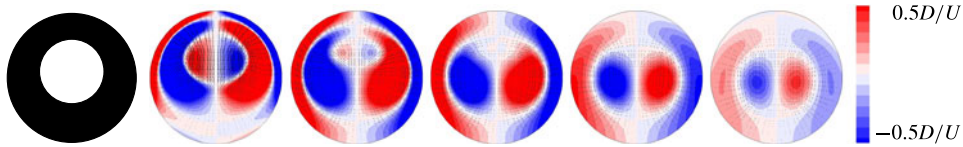

FIGURE 5. Predicted streamwise vorticity shown in axial cross-sections at $x/D = 2, 4, 6, 8$ and 10, left to right, for flow through the eccentric stenosis $E = 0.05$, for $Re = 300$.

with the jet attaching to the pipe wall. Also evident from figure 5 is the helical secondary flow generated by the eccentricity. A counter-rotating vortex pair sits near the centre of the pipe.

As the geometry eccentricity is decreased from $E = 0.05$, the deflection of the flow from the centreline of the pipe decreases. However, an order-of-magnitude reduction in the eccentricity results in a still noticeably non-axisymmetric wake flow. Only for an eccentricity as small as $E = 0.001$ does the flow regain something approaching axisymmetry to the naked eye. The skewness of the flow can be quantified using the normalized first moment of the axial velocity, defined as:

$$\mu_z(x) = \frac{\displaystyle\int\int \left(\frac{z}{D_x}\right) \frac{u}{U} \, dy \, dz}{\displaystyle\int\int \frac{u}{U} \, dy \, dz}, \tag{3.1}$$

where the integral is over the local cross-section of the pipe and D_x is the local pipe diameter. Figure 6(a) plots the variation of $\mu_z(x)$ for a range of eccentricities and for $Re = 350$. The skewness introduced by the stenosis offset can be seen in
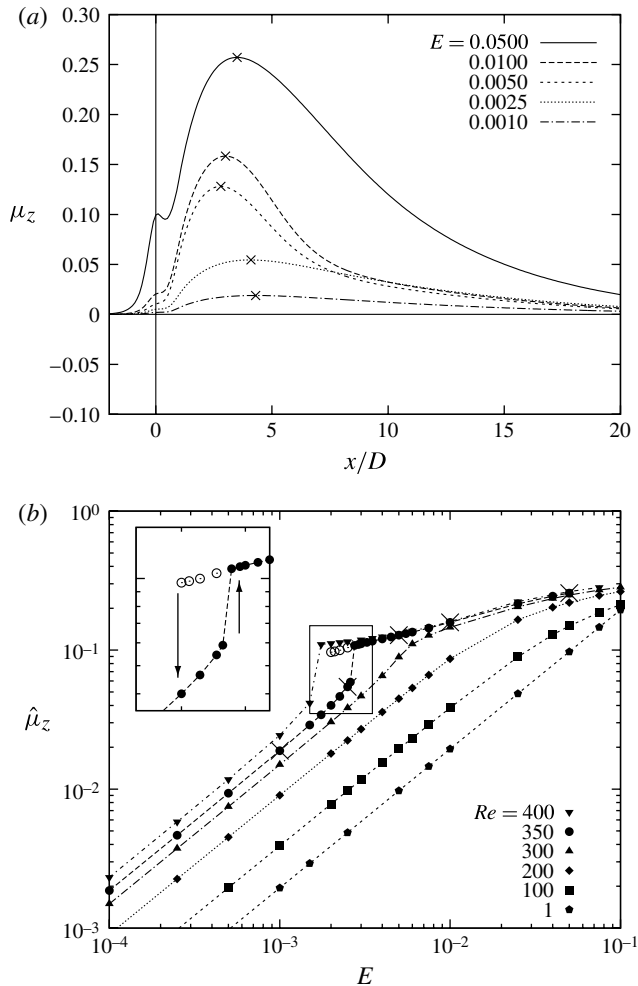
FIGURE 6. (*a*) Plots of variation of μ_z with x, for $Re = 350$ and a range of eccentricities; the crosses mark the maximum of each curve, $\hat{\mu}_z$, which, in (*b*), is plotted across the eccentricity and Reynolds number parameter space. The hollow symbols represent solutions for $Re = 350$, which were initialized with the solution from a larger eccentricity, rather than from rest. Inset, the hysteresis observed for $Re = 350$ is highlighted.

the value of μ_z at the stenosis throat, at $x/D = 0$, which scales linearly with the eccentricity. Each plot shows a maximum at approximately $x/D \approx 3.5$. Figure 6(*b*) quantifies the non-axisymmetry, by plotting the variation of this maximum, $\hat{\mu}_z$, with eccentricity, across a range of Reynolds numbers. It is reasonable to expect $\hat{\mu}_z$ to scale with the observed non-axisymmetry, such as in figure 4, and indeed this is the case. For the lower Reynolds numbers and eccentricities of the parameter space, $\hat{\mu}_z$ increases linearly with eccentricity. For larger eccentricities and Reynolds numbers, the behaviour is more complicated. For $Re = 350$, at $E = 0.0025$, there is a change in the variation of $\hat{\mu}_z$, with a tendency towards a different mode of non-axisymmetry in the flow. The results for $Re = 350$ were analysed more closely and a hysteresis loop

FIGURE 7. Two isosurfaces of axial velocity ($u/U = -0.5$ and 2.0) for the flow at Reynolds number $Re = 350$ and eccentricity $E = 0.0025$. (*a*) The weakly skewed solution, obtained from rest, and (*b*) the more strongly skewed, obtained by initializing the flow with a solution from a larger eccentricity.

was detected, which is highlighted in the inset figure. For $0.002 < E < 0.003$, two solutions are present, one with a greater wake skewness than the other. Figure 7 shows isosurfaces of axial velocity for each of the two solutions obtainable for an eccentricity of $E = 0.0025$. There are no obvious differences between the two solutions, other than one being more skewed than the other. The less skewed solution is found when the simulation is started from the flow at rest. The solution with the stronger skewness can be obtained by initializing the simulation with a solution from larger eccentricity. In this way, for $Re = 350$, the strongly skewed solution can be obtained for eccentricities down to $E = 0.002$. Further grid resolution checks were performed for these cases, and the hysteretic behaviour persists independently of greater mesh resolution.

Vétel *et al.* (2008) have taken detailed three-component SPIV measurements of the flow in the axisymmetric case, with $E = 0$; these results are the most useful for comparison with the numerical results. In interpreting figures 4 and 6, the dimensional scale and the manufacturing precision of the experimental rigs used for the results reported in Vétel *et al.* (2008) should be considered. The rig comprised a pipe of diameter 20 mm, with a stenosis test-section manufacturing precision of 0.025 mm, or $0.00125D$. Additionally, the experimental rig consisted of more than 3 m of nominally straight pipe upstream and downstream of the test-section. Some degree of misalignment is inevitable, for example from moving the test-section through the SPIV measurement apparatus.

Figure 8 compares the experimental results taken from Vétel *et al.* (2008) for flow in nominally axisymmetric geometries and the present numerical results for geometries of small eccentricity. Making a comparison between the cross-sections in figure 8(*a*) and the corresponding result in Vétel *et al.* (2008), a strong qualitative similarity can be seen. Of the three, the similarity is strongest in the numerical simulation for $E = 0.0025$. Vétel *et al.* (2008) also provided velocity profiles in their figure 6(*b*), corresponding to the straight dashed lines in our figure 8(*a*). Figure 8(*b*) presents a comparison of these velocity profiles with those of the numerical simulations for an eccentricity $E = 0.0025$. The comparison shows the same similarity seen in figure 8(*a*); the flows share a strong resemblance, but are not identical: the non-axisymmetry seen numerically is caused by a well-defined and controlled geometric eccentricity, while the non-axisymmetry seen experimentally could be caused by a number of factors. Vétel *et al.* (2008) observed changes in the direction of deflection from one run to the next. As they themselves point out, this was probably due to misalignment of the pipe, which may have changed as the test-section was moved through their SPIV measurement apparatus. In experimental work carried out by
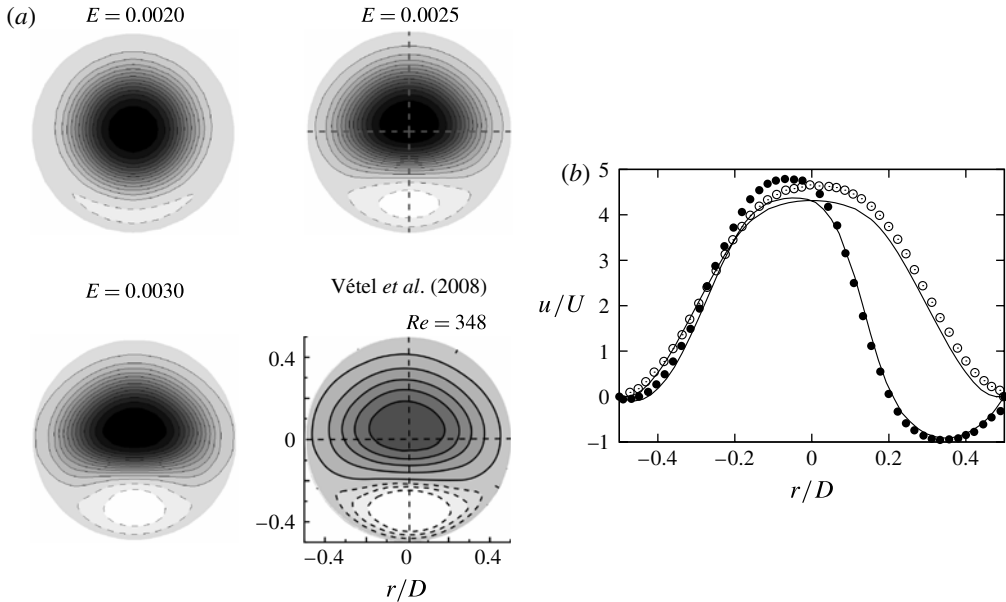
FIGURE 8. (*a*) Contours of predicted streamwise velocity for $Re = 350$, for flow in stenoses of eccentricities $E = 0.0020, 0.0025$ and 0.0030, in cross-sections at an axial station of $x/D = 3.5$. Contours in the range $-0.67 \leqslant u/U \leqslant 4$. The fourth image is an experimental result taken from figure 6(*a*) of Vétel *et al.* (2008) (contours unknown) and corresponds to $Re = 348$ and the same axial station, but a nominally axisymmetric stenosis geometry ($E = 0$). Solid lines denote positive contours, and dashed, negative. The plots have been aligned with the stenosis throat offset in the upwards direction of each image, except the image from Vétel *et al.* (2008), which has been rotated here for better comparison. The flow for $E = 0.0020$ is the weakly skewed solution of figure 6(*b*), while the the other two are the strongly skewed solution. (*b*) Comparison of velocity profiles between the present numerical simulations for $E = 0.0025$ (solid lines) and the experimental data of Vétel *et al.* (2008) (points, taken from their figure 6*b*). The data correspond to the straight dashed lines plotted in (*a*).

the authors of the current paper (Griffith *et al.* 2008, 2010), the flow through a nominally axisymmetric stenotic geometry was found to have a sensitivity to the temperature of the fluid that surrounded the pipe. Temperature differences between the fluids on either side of the pipe wall led to buoyancy effects inside the pipe, where fluid settled in the recirculation zone downstream of the stenosis was heated or cooled to a temperature different to that of the fluid arriving from upstream. The temperature of the surrounding fluid could influence the direction of the deflection of the jet.

Another potential source of misalignment is skewness on the upstream velocity profile. Peterson & Plesniak (2008) experimentally investigated stenotic flow with added upstream skewness (although for a pulsatile inlet velocity profile), which showed a tendency for the wake jet to attach to the pipe wall. Their upstream skewness was large, with the perturbed velocity profile having a peak axial velocity at a radius of $y/D \approx 0.4$; numerically, the perturbation and sensitivity can be quantified.
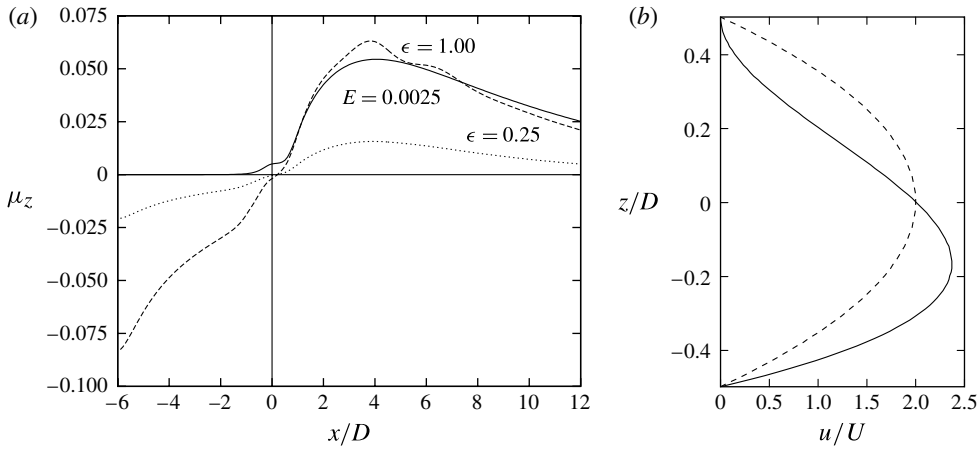
FIGURE 9. (*a*) For $Re = 350$, a comparison of profile distortion measured by μ_z with downstream distance for axisymmetric cases with $\epsilon = 0.25$ and 1.0 and the eccentric case for $E = 0.0025$. (*b*) The perturbed inflow velocity profile for $\epsilon = 1.0$. The unperturbed symmetric velocity profile (dashed line) is shown for comparison.

Consider the case of purely axisymmetric geometry, $E = 0$, but with a perturbed inflow velocity, such that

$$u(y, z) = \left(2 - 8 \left(\frac{y^2 + z^2}{D^2}\right)\right) \left(1 - 2\epsilon \frac{z}{D}\right). \tag{3.2}$$

The first term is the normal parabolic Poiseuille inlet profile and the second term a distortion which skews the distribution in the negative z-direction. The second multiplier does not affect the mean velocity, which is unity with this non-dimensionalization. Figure 9(*a*) plots the skewness, μ_z, as a function of downstream distance for two values of the inflow perturbation parameter, $\epsilon = 0.25$ and 1.0 and for the eccentric stenosis case for $E = 0.0025$, all for $Re = 350$. For the eccentric case, there is minimal perturbation to the otherwise axisymmetric velocity profile upstream of the stenosis throat, but a substantial effect downstream. The two cases with axisymmetric stenoses and a perturbed inflow show that the skewness of the velocity profile across the pipe decreases almost linearly towards the throat, where the skewness attains very small values. Downstream of the throat, the skewness variation corresponding to the large value of $\epsilon = 1.0$ is similar to that for the eccentric $E = 0.0025$ case. A geometric perturbation corresponding to $E = 0.0025$ has a similar downstream effect (at $x/D = -6$) to a much larger inflow velocity perturbation corresponding to $\epsilon = 1.0$. The large difference in level of perturbation can be seen in figure 9(*b*), showing the (strongly) perturbed inflow velocity profile which leads to a similar downstream flow as the (weakly) eccentric case of $E = 0.0025$. The presence of the contraction appears to strongly suppress the particular upstream perturbation tested; it is unknown what effect the stenosis would have on other types of upstream perturbation. Mao, Blackburn & Sherwin (2012) used transient growth analysis to find optimal perturbations to the inlet velocity profile for the axisymmetric

configuration of the current geometry. These perturbations are more complex than the skewed profile tested here and result in substantial transient growth downstream of the stenosis throat. The magnitude required for these optimal perturbations to achieve a downstream effect of similar order to the skewed velocity profile perturbation tested here is unknown for now.

The question of sensitivity to eccentricity and inlet perturbations has also been addressed in the literature for the flow in both planar and axisymmetric sudden expansions. For the planar expansion and its symmetry-breaking bifurcation, Fearn *et al.* (1990) experimentally observed asymmetric flows biased to one side of the channel. Numerically, they observed the same behaviour when a small geometric perturbation was added to their geometry (their figure 9). For the axisymmetric expansion, in a detailed transient growth and global mode stability analysis, Cantwell *et al.* (2010) and Sanmiguel-Rojas *et al.* (2010) found nothing to explain why symmetry breaking was observed experimentally for such low Reynolds numbers. Sanmiguel-Rojas & Mullin (2012) investigated numerically the effect of skewness on the inlet Poiseuille profile and found qualitative agreement between their distorted inlet numerical results and experimental results. This is in contrast to the behaviour of the stenotic flow, where the presence of the contraction in the stenosis geometry strongly suppresses any upstream perturbation to the inlet profile. Sanmiguel-Rojas & Mullin (2012) tested a single case with a geometric offset between the inlet and outlet sections and found a wake state similar to that achieved with a similar level of inlet perturbation.

Another flow phenomenon bearing some similarity is that of the asymmetry observed in vortex breakdown bubbles in the flow in a closed cylinder with a rotating end-cover. Experimentally, asymmetries are observed in the flow (Spohn, Mory & Hopfinger 1998) at Reynolds numbers lower than predicted numerically (Sorensen & Christensen 1995). Thompson & Hourigan (2003) showed that small errors in the rotating end-cover produced surprisingly strong asymmetries in the flow, a finding supported with fully three-dimensional numerical simulations in Brons *et al.* (2007). Further work showed that the accuracy of injection of visualization dye in experiments was itself sufficient to give rise to asymmetric flow (Brons, Thompson & Hourigan 2009).

4. Conclusions

Numerical simulations performed on stenoses with precisely controlled eccentricities reveal a strong sensitivity of the wake flow to misalignments in the test-section. Simulations undertaken on geometries with eccentricities of similar magnitude to the machining precision of sections used experimentally exhibit downstream jet deflections strongly similar to those observed experimentally for nominally axisymmetric geometries. By contrast, a similar magnitude perturbation consisting of an added skewness to the inlet velocity profile was found to have a significantly smaller effect on the downstream wake, due to the damping effect of the stenosis contraction. The sensitivity to eccentricity accounts for the bifurcation to a non-axisymmetric state observed experimentally for some Reynolds numbers. It indicates that achieving axisymmetric stenotic flow states experimentally for Reynolds numbers greater than 250 and below the onset of turbulence requires a high-precision machining of the test-section.

Acknowledgements

References

AHMED, S. A. & GIDDENS, D. P. 1983 Velocity measurements in steady flow through axisymmetric stenoses at moderate Reynolds numbers. *J. Biomech.* **16**, 505–516.

BRONS, M., SHEN, W. Z., SORENSEN, J. N. & ZHU, W. J. 2007 The influence of imperfections on the flow structure of steady vortex breakdown bubbles. *J. Fluid Mech.* **578**, 453–466.

BRONS, M., THOMPSON, M. C. & HOURIGAN, K. 2009 Dye visualization near a three-dimensional stagnation point: application to the vortex breakdown bubble. *J. Fluid Mech.* **622**, 177–194.

CANTWELL, C. D., BARKLEY, D. & BLACKBURN, H. M. 2010 Transient growth analysis of flow through a sudden expansion in a circular pipe. *Phys. Fluids* **22**, 034101.

FEARN, R. M., MULLIN, T. & CLIFFE, K. A. 1990 Nonlinear flow phenomena in a symmetric sudden expansion. *J. Fluid Mech.* **211**, 595–608.

GRIFFITH, M. D., LEWEKE, T., THOMPSON, M. C. & HOURIGAN, K. 2008 Steady inlet flow in stenotic geometries: convective and absolute instabilities. *J. Fluid Mech.* **616**, 111–133.

GRIFFITH, M. D., THOMPSON, M. C., LEWEKE, T. & HOURIGAN, K. 2010 Convective instability in steady stenotic flow: optimal transient growth and experimental observation. *J. Fluid Mech.* **655**, 504–514.

GRIFFITH, M. D., THOMPSON, M. C., LEWEKE, T., HOURIGAN, K. & ANDERSON, W. P. 2007 Wake behaviour and instability of flow through a partially blocked channel. *J. Fluid Mech.* **582**, 319–340.

KARNIADAKIS, G. E. & SHERWIN, S. J. 1999 *Spectral/hp Element Methods for CFD*, 1st edn. Oxford University Press.

MAO, X., BLACKBURN, H. M. & SHERWIN, S. J. 2012 Optimal inflow boundary condition perturbations in steady stenotic flow. *J. Fluid Mech.* **705**, 306–321.

PETERSON, S. D. & PLESNIAK, M. W. 2008 The influence of inlet velocity profile and secondary flow on pulsatile flow in a model artery with stenosis. *J. Fluid Mech.* **616**, 263–301.

SANMIGUEL-ROJAS, E. & MULLIN, T. 2012 Finite-amplitude solutions in the flow through a sudden expansion in a circular pipe. *J. Fluid Mech.* **691**, 201–213.

SANMIGUEL-ROJAS, E., DEL PINO, C. & GUTIÉRREZ-MONTES, C. 2010 Global mode analysis of a pipe flow through a 1:2 axisymmetric sudden expansion. *Phys. Fluids* **22**, 071702.

SHERWIN, S. J. & BLACKBURN, H. M. 2005 Three-dimensional instabilities of steady and pulsatile axisymmetric stenotic flows. *J. Fluid Mech.* **533**, 297–327.

SORENSEN, J. N. & CHRISTENSEN, E. A. 1995 Direct numerical simulation of rotating fluid flow in a closed cylinder. *Phys. Fluids* **7**, 764–778.

SPOHN, A., MORY, M. & HOPFINGER, E. J. 1998 Experiments on vortex breakdown in a confined flow generated by a rotating disc. *J. Fluid Mech.* **370**, 73–99.

THOMPSON, M. C. & HOURIGAN, K. 2003 The sensitivity of steady vortex breakdown bubbles in confined cylinder flows to rotating lid misalignment. *J. Fluid Mech.* **496**, 129–138.

VARGHESE, S. S., FRANKEL, S. H. & FISCHER, P. F. 2007 Direct numerical simulation of stenotic flows. Part 1. Steady flow. *J. Fluid Mech.* **582**, 253–280.

VÉTEL, J., GARON, A., PELLETIER, D. & FARINAS, M.-I. 2008 Asymmetry and transition to turbulence in a smooth axisymmetric constriction. *J. Fluid Mech.* **607**, 351–386.